

Supporting Information

High resolution X-ray imaging from near unity emission organic-inorganic manganese bromide scintillator film with suction filtration method

*Mengyue Wu, Jun'an Lai, *Yayun Pu, Zixian Wang, Faguang Kuang, Yongqiang Zhou,
Kang An, Sijun Cao, Baofei Sun, Zhengzheng Liu, Juan Du, Heng Luo, Peng He, *
Xiaosheng Tang **

Table S1. Crystal structure parameters of $(C_{21}H_{22}P)_2MnBr_4$

Formula	$(C_{21}H_{22}P)_2MnBr_4$
Temperature(K)	273
Mr	985.29
Crystal system	Monoclinic
Space group	P2 ₁ /n
a(Å)	17.316(4)
b(Å)	14.982(3)
c(Å)	18.264(3)
α (deg)	90
β (deg)	116.307(7)
γ (deg)	90
V(Å ³)	4247.8(16)
Z	4
ρ_{cale} (g cm ⁻³)	1.541
F (000)	1964.0
Gof on F ² (S)	1.025
R[$I > 2\sigma(I)$]	0.0609
wR ₂ (all data)	0.2071

Table S2. Bond length and bond angle of $(C_{21}H_{22}P)_2MnBr_4$ crystal cell

Bond	Length(Å)	Bond	Angle($^{\circ}$)
Mn05-Br01	2.4931(13)	Br01-Mn05-Br02	112.85(5)
Mn05-Br02	2.5369(11)	Br01-Mn05-Br03	108.55(4)
Mn05-Br03	2.5058(12)	Br01-Mn05-Br04	105.60(4)
Mn05-Br04	2.4675(11)	Br02-Mn05-Br03	112.31(4)
		Br02-Mn05-Br04	110.07(4)
		Br03-Mn05-Br04	107.08(5)

Table S3. Comparison of luminescence parameters of organic and inorganic Mn-based halides: comparison of emission wavelength (λ_{em}), PLQY, luminescence lifetime (τ) and shortest Mn-Mn distance ($d_{\text{Mn-Mn}}$).

Compound	$\lambda_{\text{em}}(\text{nm})$	PLQY(%)	$\tau(\text{ms})$	$d_{\text{Mn-Mn}}(\text{\AA})$	Ref.
$(\text{C}_{21}\text{H}_{22}\text{P})_2\text{MnBr}_4$	511	98.93	0.380	11.15	This work
$(\text{MTP})_2\text{MnBr}_4$	516	99.5	0.331	10.41	¹
$(\text{BTEA})_2\text{MnBr}_4$	521	97.8	0.346	9.17	²
$(\text{Tpp})_2\text{MnBr}_4$	520	98	0.265	10.38	³
$(\text{C}_{24}\text{H}_{20}\text{P})_2\text{MnBr}_4$	520	85	0.316	--	⁴
$(\text{C}_{10}\text{H}_{16}\text{N})_2\text{MnBr}_4$	518	89	0.330	9.18	⁵
$(\text{C}_8\text{H}_{20}\text{N})_2\text{MnBr}_4$	515	85	0.443	10.28	⁶
$(\text{C}_5\text{H}_6\text{N})_2\text{MnBr}_4$	521	95	0.261	--	⁷
$(\text{Ph}_4\text{P})_2\text{MnBr}_4$	516	98	0.355	--	⁸
$(\text{C}_{20}\text{H}_{20}\text{P})_2\text{MnBr}_4$	523	94	0.312	9.72	⁹

Table S4. Summary of X-ray scintillation performance of lead-free organic-inorganic hybrid scintillation screens.

Scintillators	Light yield (Photons MeV ⁻¹)	Detection limit (nGy s ⁻¹)	Imaging materials	Spatial resolution (lp mm ⁻¹)	Ref.
(C ₂₁ H ₂₂ P) ₂ MnBr ₄	46,786	217.7	@PVDF film	20	This work
(C ₈ H ₂₀ N) ₂ MnBr ₄	24,000	24.2	Rigid film	5.0	⁶
(C ₂₄ H ₂₀ P) ₂ MnBr ₄	/	608.0	@TPU film	14.5	⁴
(C ₂₂ H ₂₂ O ₂ P) ₂ MnBr ₄	32,000	18.0	@PMMA film	4.4	¹⁰
(DIET) ₃ Cu ₃ Br ₃	20,000	189.0	@PDMS film	11.7	¹¹
(C ₃₈ H ₃₄ P) ₂ MnBr ₄	80,000	72.8	@PDMS film	0.3mm	¹²
(TBA)CuBr ₂	24,000	/	@PVDF film	166.0μm	¹³
(BTPP) ₂ MnBr ₄	53,000	89.9	@PDMS film	10.1	¹⁴
(BTPP) ₂ MnBr ₄	23,000	74.6	@PDMS film	14.1	¹⁴

Table S5. The parameter of ISO 19232 duplex-wire image quality indicator. DD: duplex wire numbers; UT: corresponding unsharpness; SRb: corresponding basic spatial resolution; d: wire diameter and spacing; LP: corresponding line pair value.

DD	UT (μm)	SRb (μm)	d (μm)	LP (lp/mm)
D4	800	400	400	1.250
D5	640	320	320	1.560
D6	500	250	250	2.000
D7	400	200	200	2.500
D8	320	160	160	3.130
D9	260	130	130	3.850
D10	200	100	100	5.000
D11	160	80	80	6.250
D12	130	63	63	7.690
D13	100	50	50	10.00
D14	80	40	40	12.50
D15	63	32	32	15.90
D16	50	25	25	20.00
D17	40	20	20	25.00

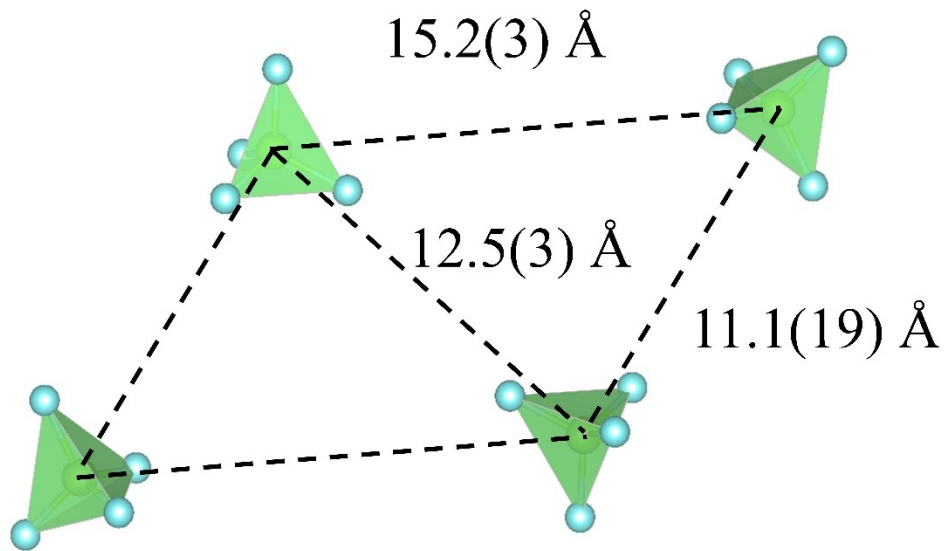


Figure S1. The $[MnBr_4]^{2-}$ tetrahedron in the crystal structure of $(C_{21}H_{22}P)_2MnBr_4$ shows the distance between adjacent Mn^{2+} ions. Distance between adjacent Mn^{2+} ions is 15.2 \AA , 12.5 \AA , and 11.1 \AA respectively.

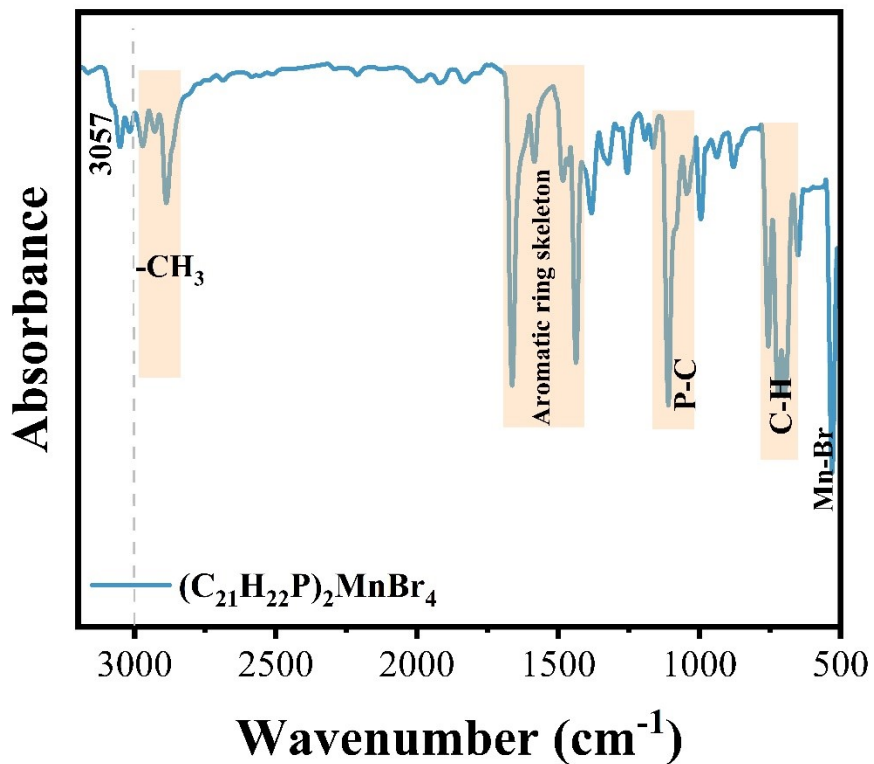


Figure S2. Fourier Transform Infrared Spectroscopy (FTIR) of the $(C_{21}H_{22}P)_2MnBr_4$ crystal.

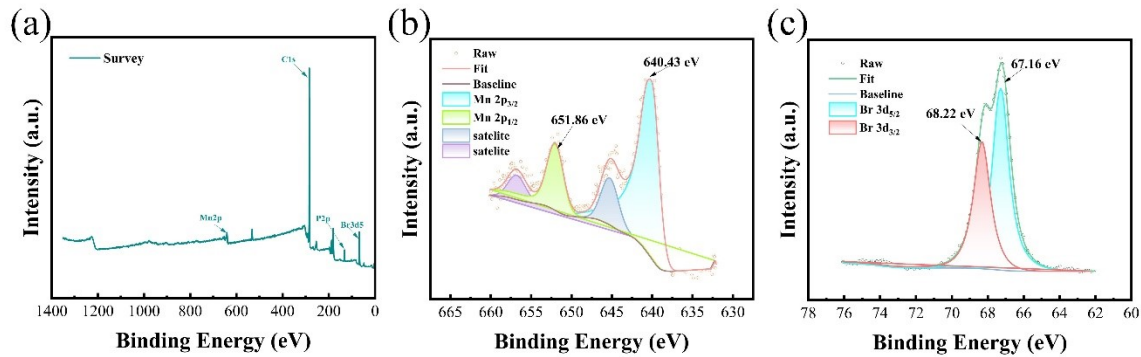


Figure S3. (a) Survey X-ray photoelectron spectrum (XPS) of $(C_{21}H_{22}P)_2MnBr_4$. There are no other impurity elements except Mn, P, Br, and C. (b) Mn and (c) Br are high-resolution Mn and Br scanning images.

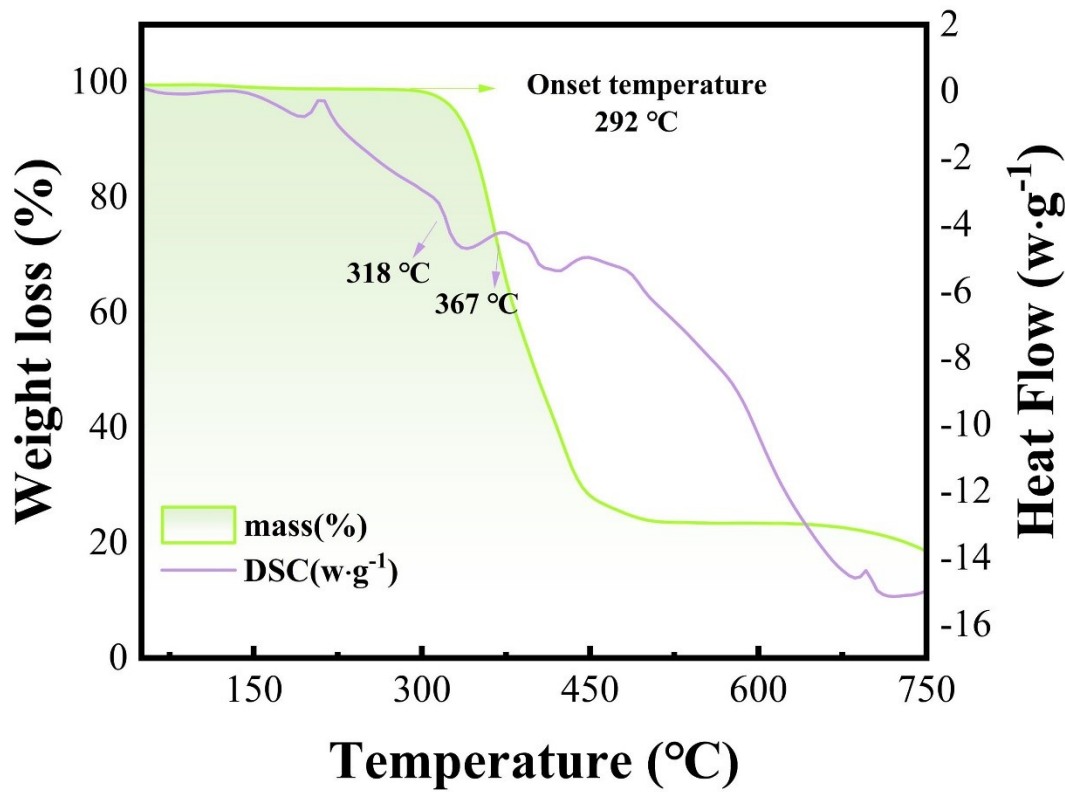


Figure S4. The TGA and DSC curves of $(\text{C}_{21}\text{H}_{22}\text{P})_2\text{MnBr}_4$ crystals. The crystal began to decompose in weightlessness at 292 degrees Celsius.

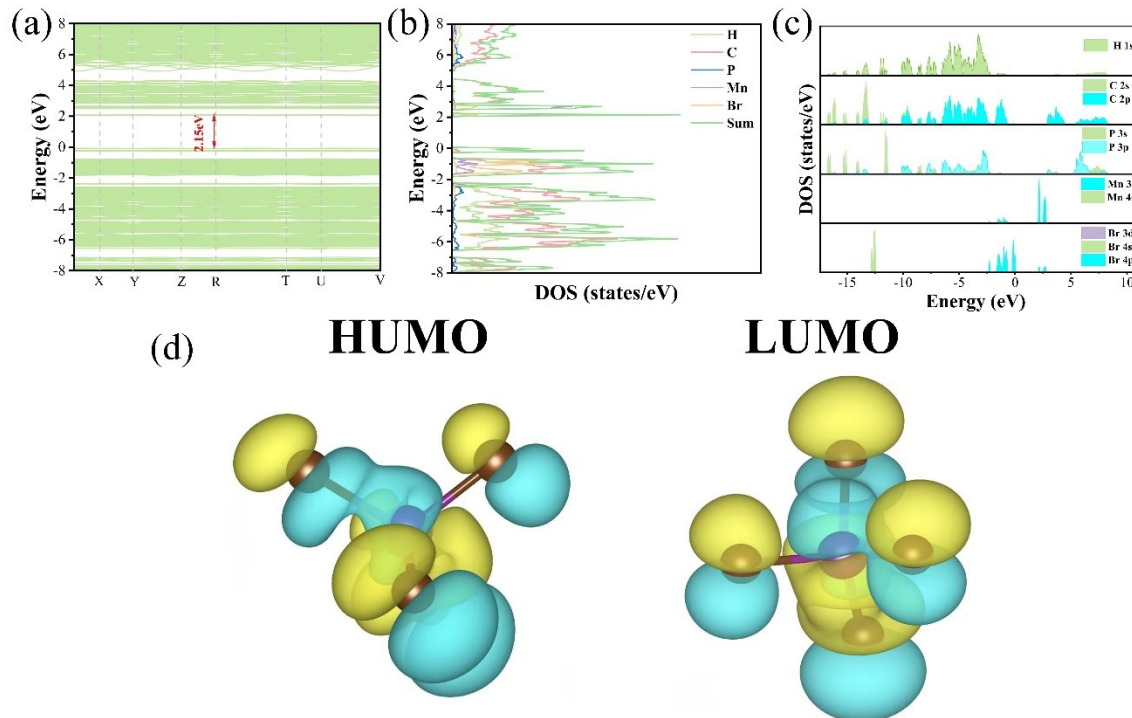


Figure S5. (a) Electronic band structure of $(C_{21}H_{22}P)_2MnBr_4$. (b) and (c) are the projected state density (PDOS) of $(C_{21}H_{22}P)_2MnBr_4$. (d) Gaussian simulated LUMO and HUMO of the $[MnBr_4]^{2-}$ tetrahedron in Compound.

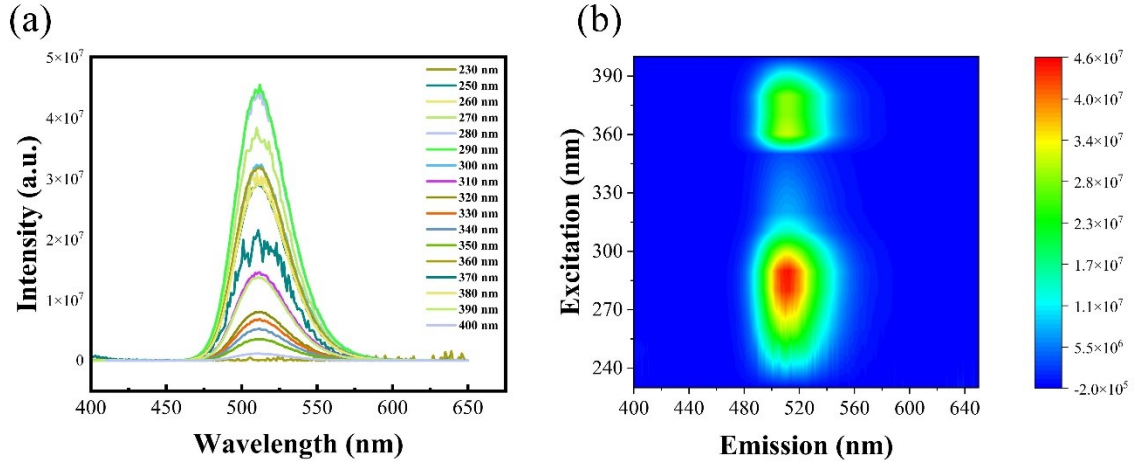


Figure S6. (a) Emission spectra (PL) of $(C_{21}H_{22}P)_2MnBr_4$ crystal under different excitation (PLE) (b) PL and PLE isolines of $(C_{21}H_{22}P)_2MnBr_4$ crystal.

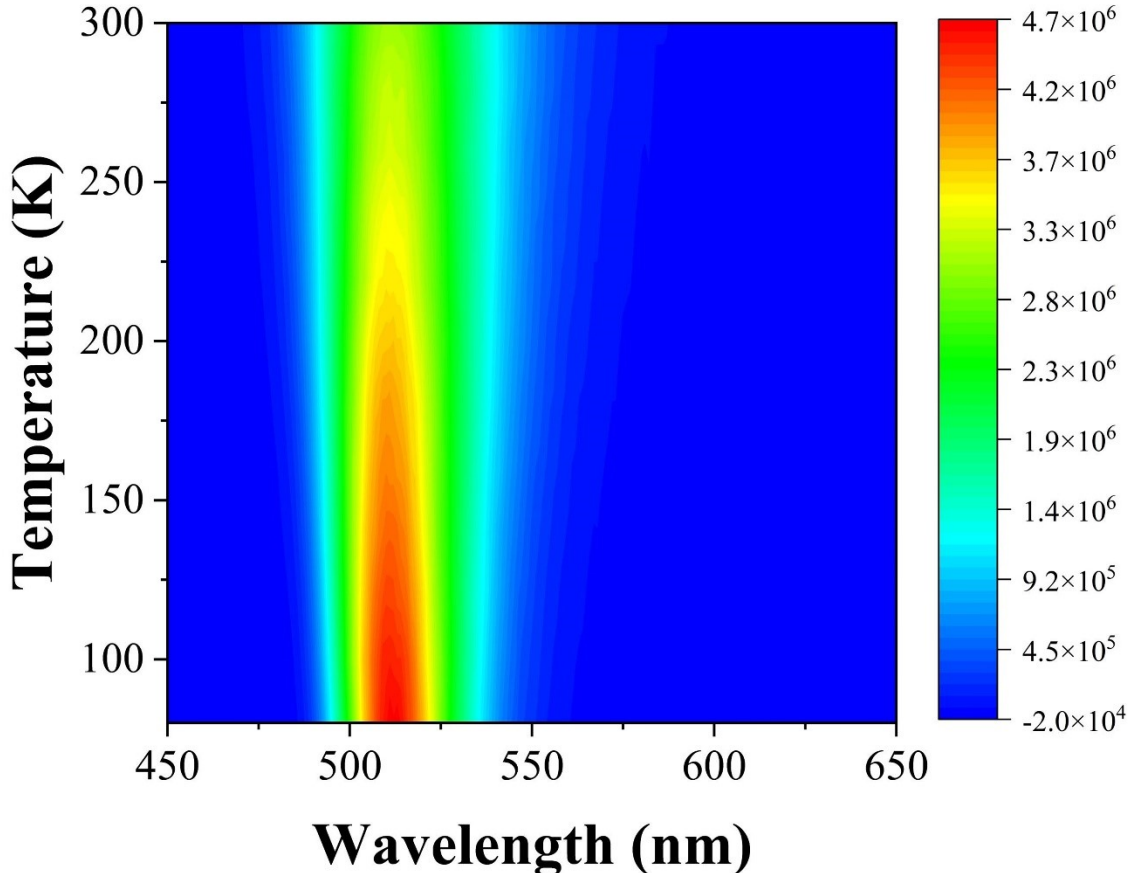


Figure S7. Temperature-dependent emissive spectrum for $(C_{21}H_{22}P)_2MnBr_4$. Illustrating the variation of FWHM (full width at half-maximum) with the temperature in the range of 80-300 K.

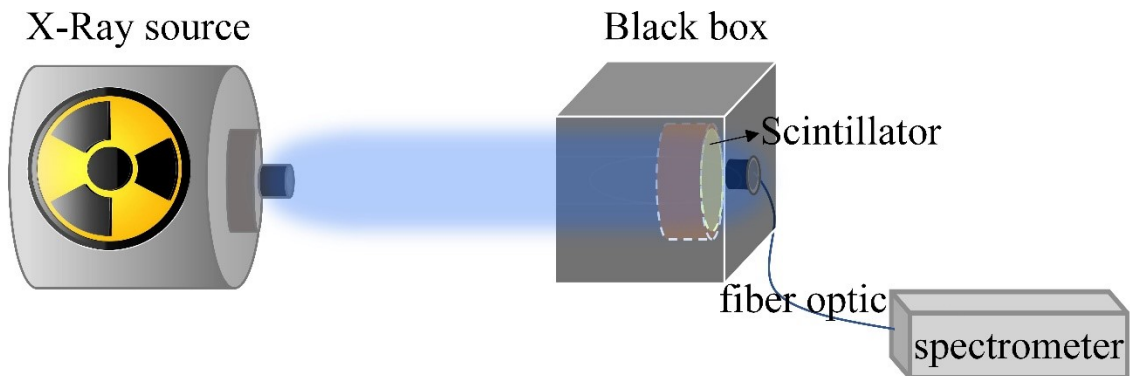


Figure S8. Schematic of the RL intensity measurement testing system.

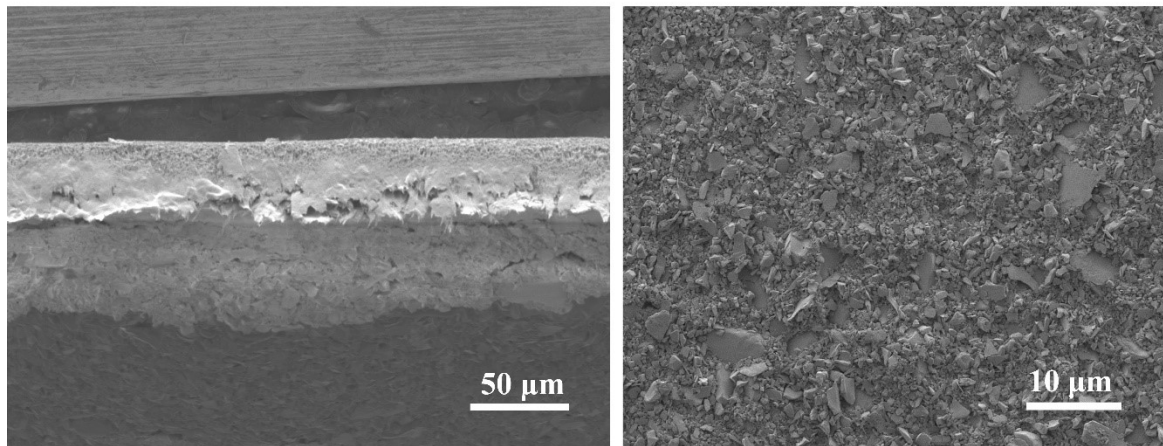


Figure S9. SEM cross-sectional view (left) and top view (right) of $(C_{21}H_{22}P)_2MnBr_4$ @PVDF film.

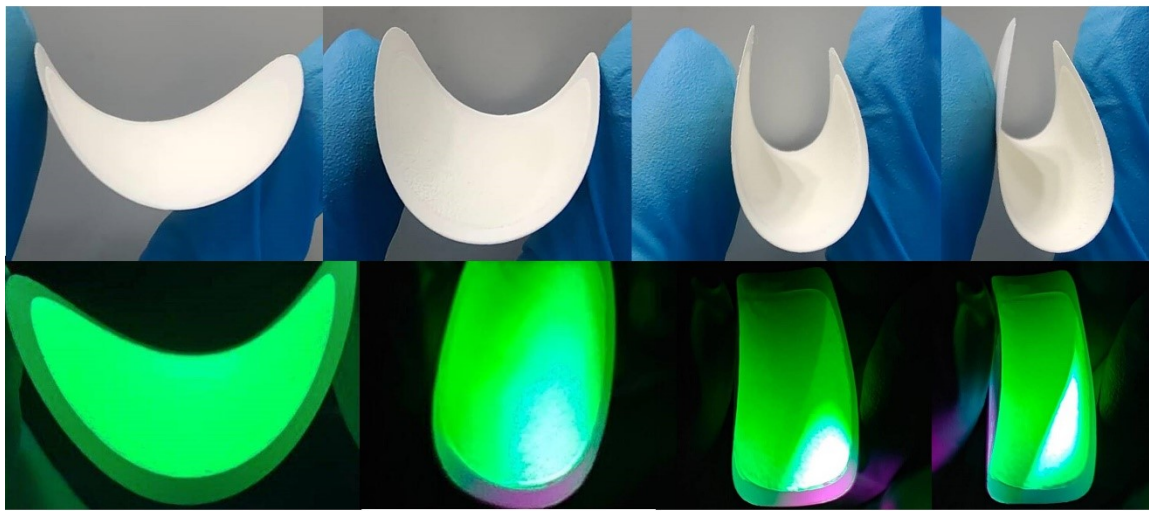


Figure S10. $(C_{21}H_{22}P)_2MnBr_4@PVDF$ scintillator film shows good flexibility under natural light and ultraviolet light.

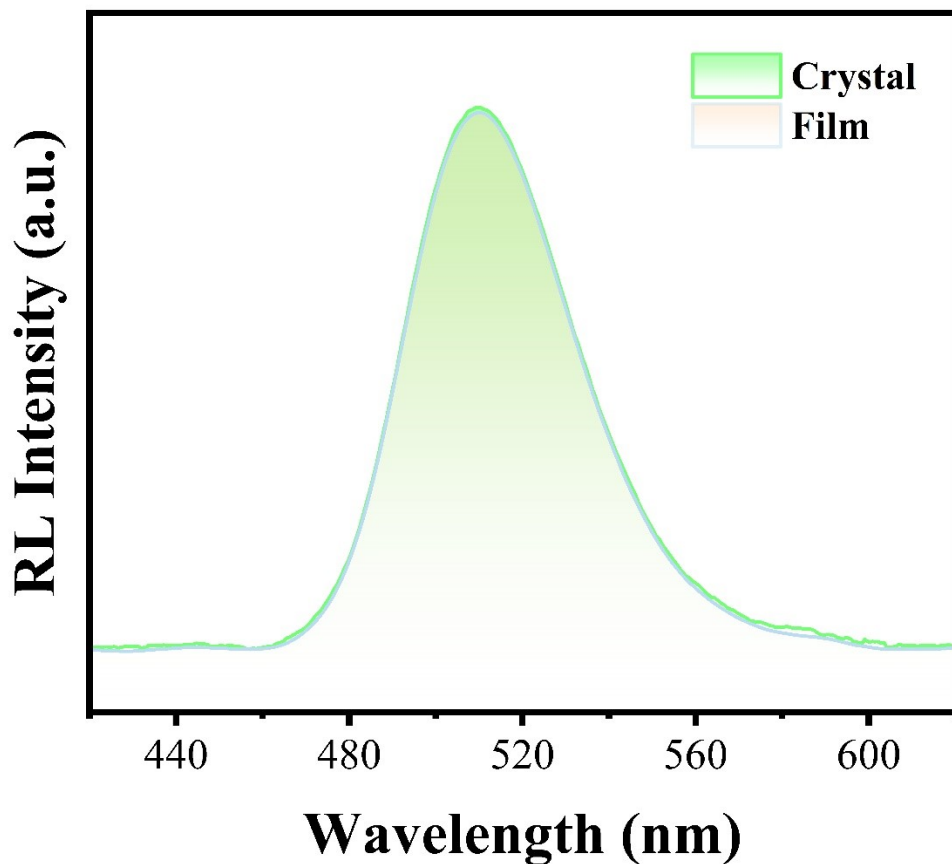


Figure S11. Comparison of RL (radioluminescence) intensity between $(C_{21}H_{22}P)_2MnBr_4$ crystal and $(C_{21}H_{22}P)_2MnBr_4@PVDF$ thin film.

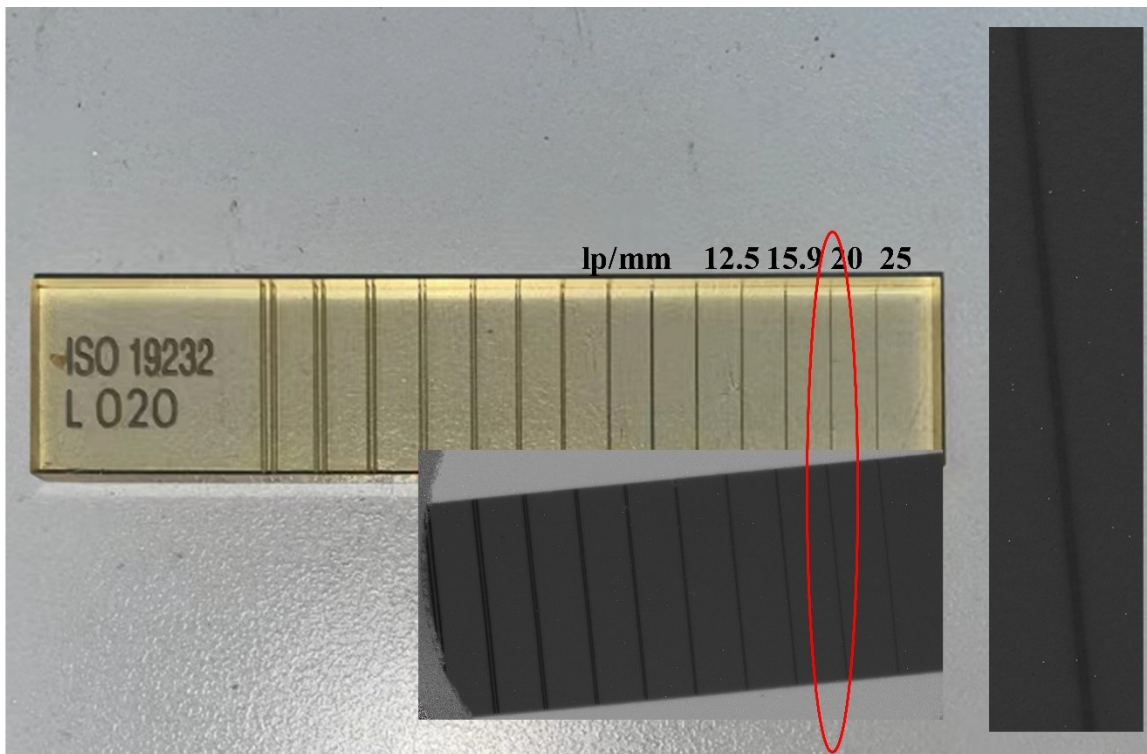


Figure S12. Physical drawing (top) and X-ray imaging drawing (bottom) of ISO 19232 standard line pair card (the inset on the right is the detailed image of the D16 line pair).

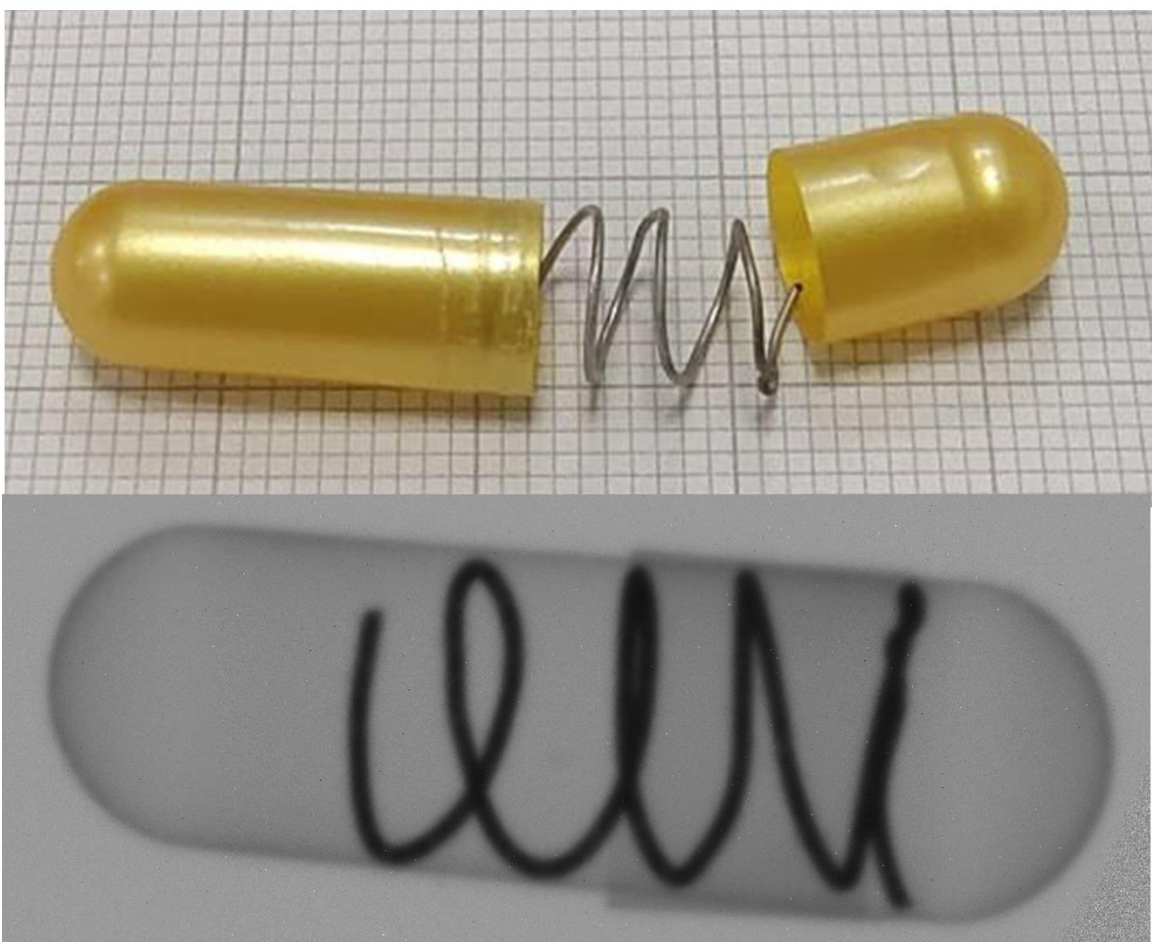


Figure S13. X-ray images of capsules under natural light and under $(C_{21}H_{22}P)_2MnBr_4$ @ PVDF scintillator film.

- 1 W. Zhang, P. Sui, W. Zheng, L. Li, S. Wang, P. Huang, W. Zhang, Q. Zhang, Y. Yu and X. Chen, Pseudo-2D Layered Organic-Inorganic Manganese Bromide with a Near-Unity Photoluminescence Quantum Yield for White Light-Emitting Diode and X-Ray Scintillator. *Angew. Chemie Int. Ed.*, 2023, **62**, e202309230.
- 2 Y. Guo, J. Wu, W. Liu and S.-P. Guo, Organic Cation Modulation Triggered Second Harmonic Response in Manganese Halides with Bright Fluorescence. *Inorg. Chem.*, 2022, **61**, 11514–11518.
- 3 K. Han, K. Sakhatskyi, J. Jin, Q. Zhang, M. V Kovalenko and Z. Xia, Seed-Crystal-Induced Cold Sintering Toward Metal Halide Transparent Ceramic Scintillators. *Adv. Mater.*, 2022, **34**, 2110420.
- 4 K. Xia, P. Ran, W. Wang, J. Yu, G. Xu, K. Wang, X. Pi, Q. He, Y. (Michael) Yang and J. Pan, In Situ Preparation of High-Quality Flexible Manganese-Halide Scintillator Films for X-Ray Imaging. *Adv. Opt. Mater.*, 2022, **10**, 2201028.
- 5 G. Zhou, Z. Liu, J. Huang, M. S. Molokeev, Z. Xiao, C. Ma and Z. Xia, Unraveling the Near-Unity Narrow-Band Green Emission in Zero-Dimensional Mn²⁺-Based Metal Halides: A Case Study of (C₁₀H₁₆N)₂Zn_{1-x}Mn_xBr₄ Solid Solutions. *J. Phys. Chem. Lett.*, 2020, **11**, 5956–5962.
- 6 T. Jiang, W. Ma, H. Zhang, Y. Tian, G. Lin, W. Xiao, X. Yu, J. Qiu, X. Xu, Y. (Michael) Yang and D. Ju, Highly Efficient and Tunable Emission of Lead-Free Manganese Halides toward White Light-Emitting Diode and X-Ray Scintillation Applications. *Adv. Funct. Mater.*, 2021, **31**, 2009973.
- 7 G. Hu, B. Xu, A. Wang, Y. Guo, J. Wu, F. Muhammad, W. Meng, C. Wang, S. Sui, Y. Liu, Y. Li, Y. Zhang, Y. Zhou and Z. Deng, Stable and Bright Pyridine Manganese Halides for Efficient White Light-Emitting Diodes. *Adv. Funct. Mater.*, 2021, **31**, 2011191.
- 8 L.-J. Xu, C.-Z. Sun, H. Xiao, Y. Wu and Z.-N. Chen, Green-Light-Emitting Diodes Based on Tetrabromide Manganese(II) Complex through Solution Process. *Adv. Mater.*, 2017, **29**, 1605739.
- 9 G. Zhou, Q. Ren, M. S. Molokeev, Y. Zhou, J. Zhang and X.-M. Zhang, Unraveling the Ultrafast Self-Assembly and Photoluminescence in Zero-Dimensional Mn²⁺-

- Based Halides with Narrow-Band Green Emissions. *ACS Appl. Electron. Mater.*, 2021, **3**, 4144–4150.
- 10 H. Meng, W. Zhu, Z. Zhou, R. Zhou, D. Yan, Q. Zhao and S. Liu, High-Efficiency Luminescent Organic–Inorganic Hybrid Manganese(II) Halides Applied to X-Ray Imaging. *J. Mater. Chem. C*, 2022, **10**, 12286–12291.
 - 11 K. Han, J. Jin, B. Su, J. Qiao and Z. Xia, Promoting Single Channel Photon Emission in Copper(I) Halide Clusters for X-Ray Detection. *Adv. Opt. Mater.*, 2022, **10**, 2200865.
 - 12 L.-J. Xu, X. Lin, Q. He, M. Worku and B. Ma, Highly Efficient Eco-Friendly X-Ray Scintillators Based on an Organic Manganese Halide. *Nat. Commun.*, 2020, **11**, 4329.
 - 13 L. Lian, X. Wang, P. Zhang, J. Zhu, X. Zhang, J. Gao, S. Wang, G. Liang, D. Zhang, L. Gao, H. Song, R. Chen, X. Lan, W. Liang, G. Niu, J. Tang and J. Zhang, Highly Luminescent Zero-Dimensional Organic Copper Halides for X-Ray Scintillation. *J. Phys. Chem. Lett.*, 2021, **12**, 6919–6926.
 - 14 W. Li, Y. Li, Y. Wang, Z. Zhou, C. Wang, Y. Sun, J. Sheng, J. Xiao, Q. Wang, S. Kurosawa, M. Buryi, D. John, K. Paurová, M. Nikl, X. OuYang and Y. Wu, Highly Efficient and Flexible Scintillation Screen Based on Organic Mn(II) Halide Hybrids toward Planar and Nonplanar X-Ray Imaging. *Laser Photon. Rev.*, 2024, **18**, 2300860.